

Supporting Info for “Translocation dynamics of knotted polymers under a constant or periodic external field”

Vivek Narsimhan,[†] C. Benjamin Renner,^{†,‡} and Patrick S. Doyle^{*,†}

[†]*Department of Chemical Engineering, Massachusetts Institute of Technology, Cambridge, MA 02139, USA*

[‡]*Current address: Liquiglide, 75 Sidney Street, Cambridge, MA 02139, USA*

E-mail: pdoyle@mit.edu

Simulation methods

We treat the polymer as a linear chain of N beads of diameter b connected by $N - 1$ rigid rods of length ℓ . In this study, $N = 200$ and we will examine three different bead diameters: touching beads ($b = \ell$), non-touching beads ($b = 0.8\ell$), and overlapping beads ($b = 1.5\ell$). If we neglect hydrodynamic interactions between chain segments, the force balance on each bead satisfies the discrete Langevin equation:

$$\mathbf{r}_i(t + \Delta t) = \mathbf{r}_i(t) + \frac{\Delta t}{\zeta} \left[T_i \mathbf{u}_i - T_{i-1} \mathbf{u}_{i-1} - \frac{\partial U}{\partial \mathbf{r}_i} + \mathbf{F}_i^{rand}(t) \right] \quad (1)$$

In the above equation, \mathbf{u}_i are the unit vectors of each bond, and T_i are the tensions that enforce the constraints of constant bond length, i.e., $|\mathbf{r}_{i+1} - \mathbf{r}_i| = \ell$ for $i = 1, \dots, N - 1$. For a linear chain, $\mathbf{u}_0 = \mathbf{u}_N = 0$ and $T_0 = T_N = 0$. The force \mathbf{F}_i^{rand} is uncorrelated white-noise that satisfies the fluctuation-dissipation theorem: $\langle \mathbf{F}_i^{rand}(t) \mathbf{F}_j^{rand}(t) \rangle = 2kT\zeta \mathbf{I} \delta_{ij} / \Delta t$,

where kT is the temperature, ζ is the friction coefficient of each bead, \mathbf{I} is the identity matrix, δ_{ij} is the Kronecker delta, and Δt is the simulation time step. Lastly, the term U is the potential energy due to the excluded volume interactions and the externally applied force. Expressions for each of these energy functions is below.

The externally applied force takes the form:

$$U_{ext} = - \sum_{pore} f(t) z_i \quad (2)$$

where $f(t)$ is a time-dependent body force and z_i is the position of bead i along the pore axis. We only sum over beads that lie inside the pore. The force profiles we examine are either a constant force or a square wave (see Fig 3a in main text).

The excluded volume interactions between polymer segments are treated as harmonic potentials between non-neighboring beads:

$$U_{EV}^{bead-bead} = \frac{H}{2} \sum_{j=1}^N \sum_{i=1}^{j-1} (r_{ij} - b + \epsilon)^2 \quad (3)$$

where r_{ij} is the distance between beads i and j , H is a spring constant, and ϵ is a small number. We only sum over beads that overlap (i.e., $r_{ij} < b$). The spring constant H tunes the softness of the excluded volume interactions – we choose $H = 5000 kT / \ell^2$ so that the beads are reasonably stiff. We note that the excluded volume interactions are the stiffest potentials in our system, so the time step of the simulation must be at least $\Delta t \sim O(\zeta/H)$ or smaller to resolve the dynamics properly. Following the ideas of Heyes and Melrose,¹ we choose $\Delta t = 0.5\zeta/H$ and $\epsilon = 10^{-3}\ell$ so that on average, two beads that are overlapping at the beginning of the time step will move slightly past contact at the end of the step.

To enforce the excluded volume interactions between the chain and the pore, we apply a similar harmonic potential between the pore wall and the beads:

$$U_{EV}^{bead-wall} = H \sum_{i=1}^N (\rho_i - \frac{b}{2} + \epsilon)^2 \quad (4)$$

where ρ_i is the distance between bead i and the pore wall. We only sum over beads that overlap with the wall (i.e., $\rho_i < 0.5b$). The pore is planar slab with a cylindrical hole of radius R and depth L . If the z axis corresponds to the center axis of the cylindrical hole, the equations for the slab's surface are given by $r = R$ for $|z| < L/2$ and $z = \pm L/2$ for $r > R$. We use the same spring constant H in the bead-bead repulsion case (i.e., $H = 5000 kT/\ell^2$). The values we choose for the pore radius and length are $R = \ell$ and $L = 10\ell$.

To update the position of the chain, we integrate eqn 1 subject to the constraints of fixed rod distance (i.e., $|\mathbf{r}_{i+1} - \mathbf{r}_i| = \ell, i = 1, \dots, N - 1$). Enforcing the constraints leads to a system of nonlinear equations for the tensions T_i ,² which we solve at each step using a modified Newton's method.³ Note: to make the statistics of the chain equivalent to that of a bead-spring chain of very large stiffness, we also add a pseudo-bending force to the Langevin equation (1),^{4,5} although we believe that this force will not make any qualitative changes to our results. Below, we discuss the initial conditions of our simulations and the knot tracking techniques we employ.

We start our simulations by introducing a knot⁶ into the center of a straight polymer and allow the knot to relax in free space for 1000 rod diffusion times, a.k.a., $t = 1000 \ell^2 \zeta / kT$. During this process, we periodically add reptation moves⁷ to fix the knot at the center of the polymer. After this process is complete, we add the pore and introduce the last monomer of the polymer into the pore region. We run the simulation for 5000 rod diffusion times or until the polymer completely translocates through the pore. We perform between 20-100 replicate simulations in order to obtain error estimates for the translocation speeds.

To measure the boundaries of the knotted region in our simulations, we employ two techniques. The first technique involves projecting the knot onto a plane parallel to the pore axis and then determining the smallest subset of crossings that retains the chain topology via computation of the Alexander polynomial.^{8,9} Since there are many planes that satisfy this condition, we choose the plane that gives rise to the smallest knot size.

When the knot is jammed at the pore wall, we can also use a simpler technique to obtain the knotted boundary. We start one bead into the pore and calculate its number of nearest neighbors, defined as the number of beads within a cutoff radius $R_{cutoff} = 1.2b$. We march left until $N_{neighbors} = 2$, at which we assign this bead as the left knot boundary. We typically use the simpler technique to calculate the knot's radius of gyration when it is jammed at the pore, although it can only be used in the situation when the knot is relatively tight.

Estimating voltage drop from the applied force

In the manuscript, we stated that a force of $f = 1 - 20 kT/\ell$ corresponds to a voltage drop of $0.20 - 4.1$ V across a pore of radius $R = b = \ell = 1$ nm and length $L = 10\ell$. We provide details of this calculation here. The method we perform is similar to the procedure outlined by van Dorp et al.¹⁰

When a single-stranded DNA moves through the pore at large forces, the strand is nearly straight inside the pore. We thus approximate the strand in this region as a cylinder of diameter b aligned with the pore axis. The polymer has a linear charge density of $\sigma_{bare} = -0.48$ nC/m and the pore wall has an areal charge density of $\sigma_{pore} = -15$ mC/m², a value that is reasonable for SiO₂ surfaces at neutral pH.¹¹ If we apply a potential ΔV across the pore, the total force on the polymer will be $F = \sigma_{bare}\Delta V + F_{eo}$, where F_{eo} is the electro-osmotic force due the flow of the counterions inside the pore. We give the expression for F below.

To determine an expression for F_{eo} , we solve for the flow field inside the pore: $\nabla_r^2 u_z = -E_z \rho(r)$, where $E_z = -\Delta V/L$ is the applied electric field and $\rho(r)$ is the charge density of the counterions in the solution. From Gauss's law of electrostatics, the density satisfies $\rho = -\frac{ekT}{\epsilon} \nabla_r^2 \tilde{\psi}$, where ϵ is the electric permittivity of water and $\tilde{\psi} = \psi e/kT$ is the reduced electrostatic potential. We solve for the velocity and obtain F_{eo} by integrating the shear stress over the strand's surface. After some algebra, the total force on the strand is:

$$F_{tot} = \frac{2\pi\epsilon kT}{e \ln(2R/b)} [\tilde{\psi}(R) - \tilde{\psi}(0.5b)] \Delta V \quad (5)$$

The force is directly proportional to the voltage drop ΔV and the radial potential difference between the pore and the strand: $[\tilde{\psi}(R) - \tilde{\psi}(0.5b)]$. Noting that $F = N_{pore}f$, where f is the force per bead and $N_{pore} = 10$ is the number of beads in the pore, we re-arrange the above formula to obtain the expression for the voltage drop:

$$\Delta V = f \frac{eN_{pore} \ln(2R/b)}{2\pi\epsilon kT [\tilde{\psi}(R) - \tilde{\psi}(0.5b)]} \quad (6)$$

Our goal is to determine the voltage drop in eqn (6) given the parameters of our problem. Unfortunately, we we must calculate the potential drop $\tilde{\psi}$ between the strand and the pore as we do not knot this quantity *a-prori*.

We determine electrostatic potential $\tilde{\psi}$ by solving the Poisson-Boltzmann equation in the pore region:

$$\nabla_r^2 \tilde{\psi} = \lambda_D^{-2} \sinh(\tilde{\psi}) \quad (7)$$

where λ_D is the Deybe screening length. For a solution of ionic strength 0.1 M in water, the value for $\lambda_D \approx 0.97$ nm. The boundary conditions for this equation are:

$$\frac{\partial \tilde{\psi}}{\partial r} = -\frac{\sigma_{bare}e}{\pi b \epsilon kT} \quad \text{at} \quad r = 0.5b \quad (8)$$

$$\frac{\partial \tilde{\psi}}{\partial r} = \frac{\sigma_{pore}e}{\epsilon kT} \quad \text{at} \quad r = R \quad (9)$$

Both equations state that the electric displacement matches the charge density at the strand and at the pore surface. We solve this boundary value problem and plug the solution into eqn (6). We obtain $\Delta V = 0.20 - 4.1$ volts across the nanopore for $f = 1 - 20 kT/\ell$ per bead. The effective charge density of the DNA inside the pore is thus

$q_{eff} = fN_{pore}/\Delta V = -0.20$ nC/m, or equivalently 42% of the charge on the bare strand. If we repeat the same calculation without any charge at the pore wall, we obtain the effective charge density to be $q_{eff} = -0.24$ nC/m, or equivalently 49% of the charge on the bare strand.

Translocation profiles – constant force

In Fig 2a of the paper, we plotted trajectories of a 4_1 -knotted polymer moving through a pore when the bead size is equal to the rod length ($b = \ell$). At low applied forces, the polymer moves at a nearly uniform speed. At high forces, the knot jams and halts the polymer's motion. At intermediate forces, the polymer's speed and transit time exhibit large fluctuations. Here, we show the trends for the other knot topologies, namely $3_1, 5_1, 5_2$, and 6_1 .

Fig S1 and S2 show trajectories with the 5_1 and 6_1 knots. For the most part, the trajectories demonstrate the same qualitative trends as the 4_1 knot. Just below the jamming transition ($f \approx 10 kT/\ell$ for 5_1 and $f \approx 7 kT/\ell$ for 6_1), the transit times exhibit a broad distribution. At larger forces, the 6_1 knot becomes practically jammed while the 5_1 knot traverses through the pore at a very small, nearly constant velocity.

Polymers with a 3_1 or 5_2 knot exhibit different trends than ones with a 4_1 knot. For example, we observe stick-slip motion for the 3_1 topology, but the fluctuations in the polymer's speed are smaller when compared to the 4_1 topology (Fig S3). For the 5_2 knot, we observe multiple regimes where the fluctuations are large. In Fig S4, we see that the polymers with a 5_2 knot move at a nearly constant speed at $f = 1 kT/\ell$. The speed has a bimodal distribution at $f = 3 kT/\ell$ and then gets back to a unimodal distribution at $f = 5 kT/\ell$. At $f = 7 kT/\ell$, some of the trajectories are jammed while others move through at a relatively constant speed. In this situation, the configuration of the knot at the pore determines the ultimate dynamics of the polymer. At very large forces ($f = 15 kT/\ell$), the

trajectories are jammed for the most part. In summary, we observe large fluctuations close to the jamming transition (see $f = 7 kT/\ell$), but observe these fluctuations at other force values as well (see $f = 3 kT/\ell$). In the future, it will be interesting to explain why this phenomenon occurs for the 5_2 topology in particular.

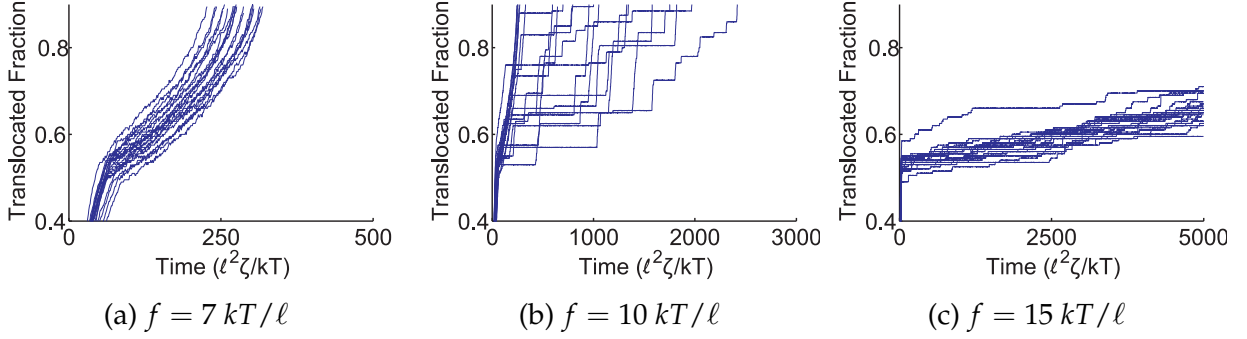


Figure S1: Translocation trajectories of a polymer with a 5_1 knot under constant force. (a) $f = 7 kT/\ell$, (b) $f = 10 kT/\ell$, (c) $f = 15 kT/\ell$. The bead size is the same as the rod length ($b = \ell$).

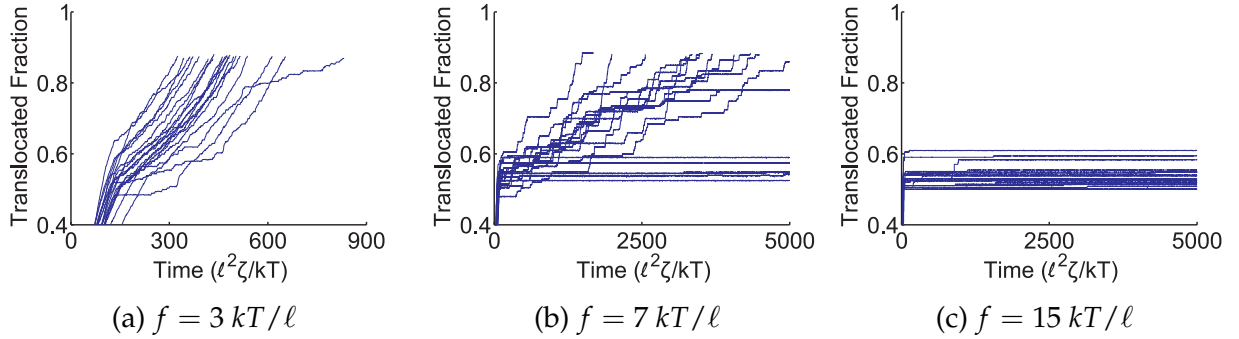


Figure S2: Translocation trajectories of a polymer with a 6_1 knot under constant force. (a) $f = 3 kT/\ell$, (b) $f = 7 kT/\ell$, (c) $f = 15 kT/\ell$. The bead size is the same as the rod length ($b = \ell$).

Translocation profiles – pulsed force field with $b = \ell$

In the main text, we found that cycling the force field at large amplitudes can enhance fluctuations in the translocation speed. This effect was observed for the 4_1 knot topology

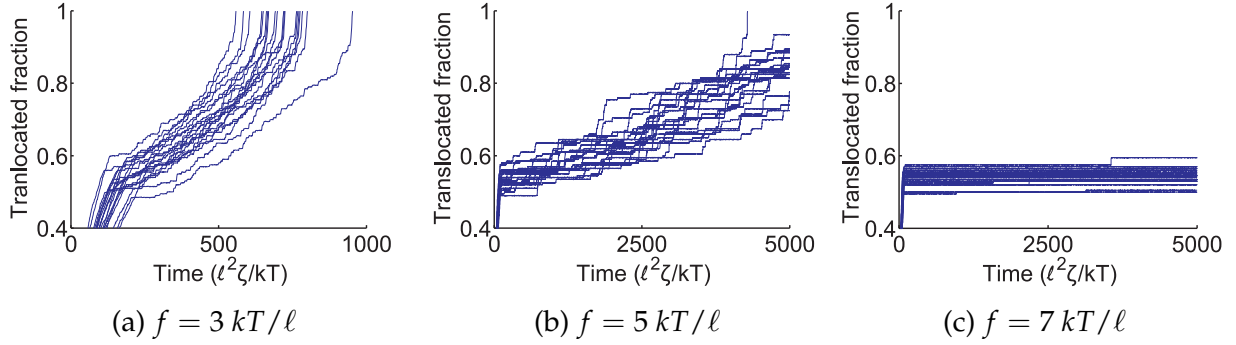


Figure S3: Translocation trajectories of a polymer with a 3_1 knot under constant force. (a) $f = 3 kT/\ell$, (b) $f = 5 kT/\ell$, (c) $f = 7 kT/\ell$. The bead size is the same as the rod length ($b = \ell$).

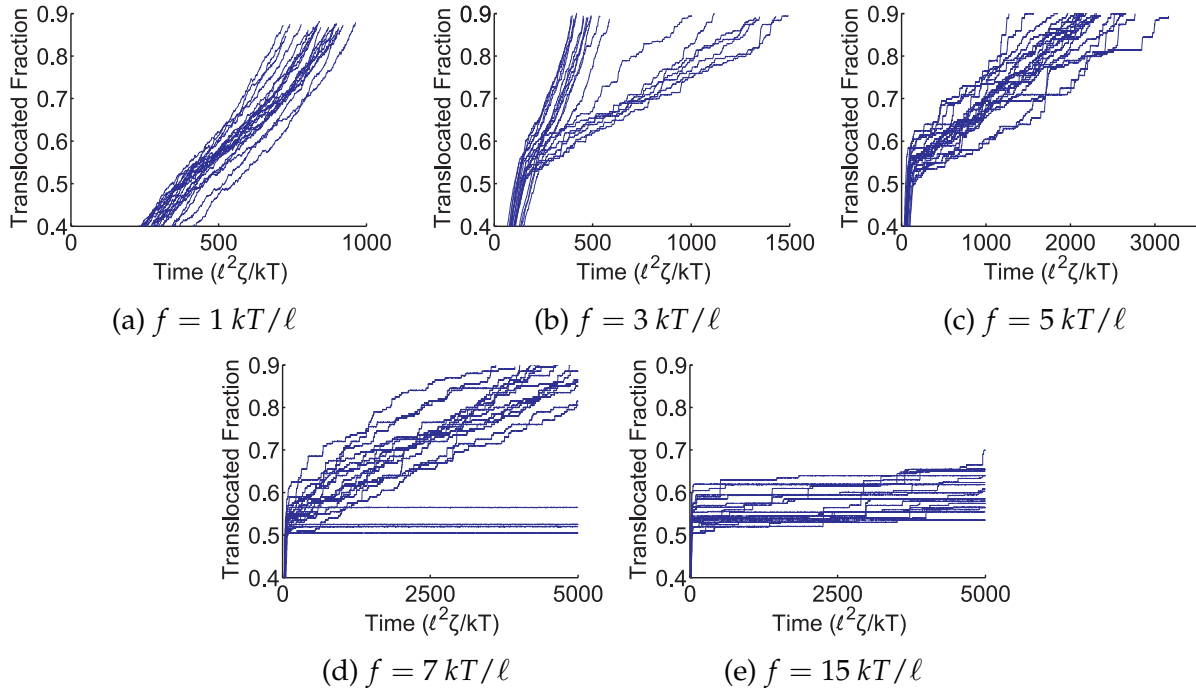


Figure S4: Translocation trajectories of a polymer with a 5_2 knot under constant force. (a) $f = 1 kT/\ell$, (b) $f = 3 kT/\ell$, (c) $f = 5 kT/\ell$, (d) $f = 7 kT/\ell$, and (e) $f = 15 kT/\ell$. The bead size is the same as the rod length ($b = \ell$).

but not for the 3_1 topology when the bead size b is equal to the rod length ℓ (see Fig 6 in text). We examine other topologies in this section.

Fig S5 shows trajectories of a 5_2 -knotted polymer and a 6_1 -knotted polymer moving through a pore under an oscillating force field. The force switches on and off with the on-time being $\tau_1 = 80 \ell^2 \zeta / kT$ and the off-time being $\tau_2 = 20 \ell^2 \zeta / kT$. At force $f = 7 kT / \ell$, both polymers ratchet through the pore at a fairly constant speed. However, if the force becomes very large ($f = 15 kT / \ell$), the 5_2 knot experiences a broad distribution in its transit times. A few trajectories of the 6_1 knot appear to be caged as well.

Unlike the 5_2 and 6_1 topologies, the 5_1 knot ratchets smoothly through the pore at these high forces (Fig S6). These dynamics are similar to what occurs for the 3_1 knot as seen in the main text (see Fig 6). Thus, based on our observations, it appears that the non-torus knots ($4_1, 5_2, 6_1$) receive enhanced fluctuations when one cycles the force field at very high amplitude. This effect is negligible for torus knots ($3_1, 5_1, 7_1$) in the range of forces we study.

In Fig S7, we examine the mechanism behind this phenomenon. Like in the main text, we run a simulation of a knotted polymer undergoing a step relaxation at the pore wall. When the initial force is very large ($f = 15 kT / \ell$), we see that the torus knots 3_1 and 5_1 swell during the relaxation process, but some of the non-torus knots ($4_1, 5_2, 6_1$) remain caged. Thus, it appears that non-torus knots are more likely to remain jammed during knot relaxation. This caging is what leads to enhanced fluctuations in the polymer's speed when we cycle the field on and off.

We close by determining how topology affects the ratcheting dynamics of a knotted polymer when the knot swells normally during relaxation (i.e., does not arrest). We cycle the force field between $f_1 = 7 kT / \ell$ and $f_2 = 0 kT / \ell$, and we set the total cycle time to be $\tau_1 + \tau_2 = 100 \ell^2 \zeta / kT$ for the twist-knot topologies we examine ($3_1, 4_1, 5_2, 6_1$). We observe similar translocation speeds for these knots (Fig S8), but the torus knots 5_1 and 7_1 do not ratchet since the forces are below the jamming transition. This result suggests that topology

is important in determining the jamming transition of the knot, but topology plays a weak role in the ratcheting behavior as long as the knot jams at the pore entrance and the knot swells normally during relaxation. Of course, this statement is only valid up to a certain point, and we fully expect topology to play a much greater role in the ratcheting dynamics for more complicated knots. This topic would be interesting to pursue in future work.

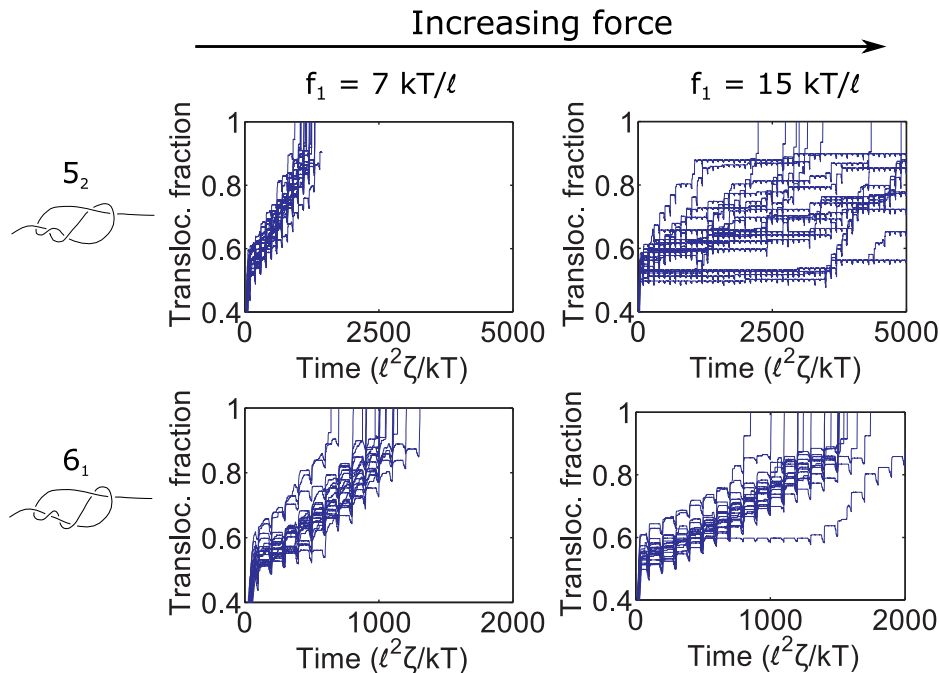


Figure S5: Ratcheting dynamics for the 5_2 and 6_1 knotted topologies. Top row: trajectories of a 5_2 -knotted polymer moving through a pore via an oscillating force field. The time of the on cycle is $\tau_1 = 80 \ell^2 \zeta / kT$, and the time of the off cycle is $\tau_2 = 20 \ell^2 \zeta / kT$. Bottom row: trajectories for a 6_1 -knotted polymer with the same cycle times. At moderate forces ($f_1 = 7 kT/\ell$), the 5_2 and 6_1 knots ratchet through the pore at a fairly constant velocity. At larger forces ($f_1 = 15 kT/\ell$), the translocation speeds start exhibiting large fluctuations. Here, the bead size is equal to the rod length ($b = \ell$).

Effect of polymer backbone corrugation on the jamming of knots

Here, we examine how the roughness along the polymer backbone alters the jamming dynamics of knots. We will examine three different corrugations from our bead-rod model:

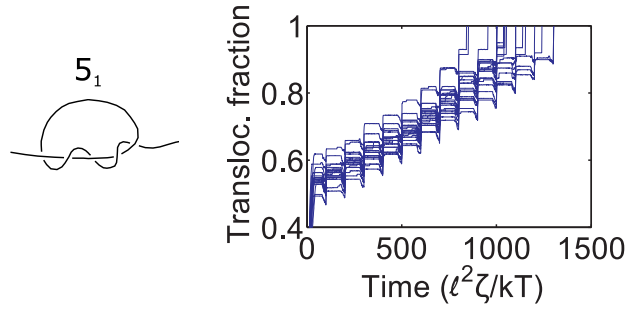


Figure S6: Ratcheting dynamics of a 5_1 -knotted polymer. The force field oscillates between force $f_1 = 15 kT/\ell$ and $f_2 = 0$. The cycle times are $\tau_1 = 80 \ell^2 \zeta/kT$ and $\tau_2 = 20 \ell^2 \zeta/kT$. The bead size is equal to the rod length ($b = \ell$).

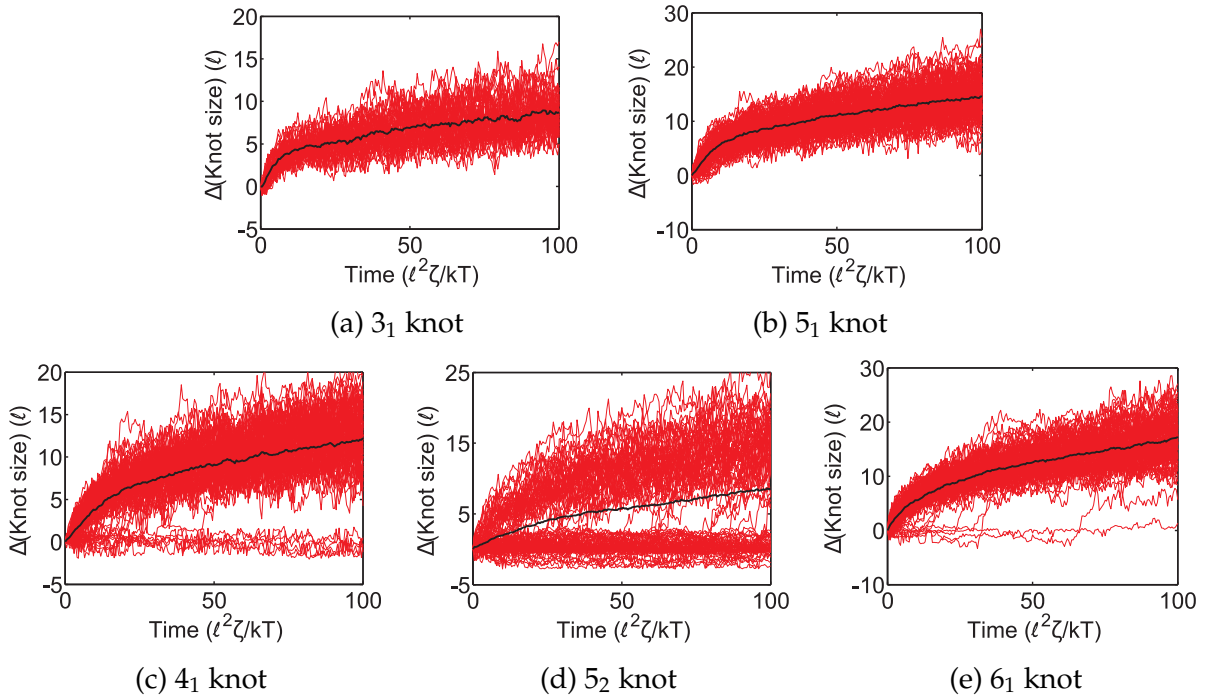


Figure S7: Knot swelling after step relation: (a) 3_1 , (b) 5_1 , (c) 4_1 , (d) 5_2 , (e) 6_1 . The initial force before relaxation is $f = 15 kT/\ell$. The black curves for each plot corresponds to the average knot swelling over 100 runs. The top row corresponds to torus knots and the bottom row corresponds to non-torus knots. The bead size is equal to the rod length ($b = \ell$).

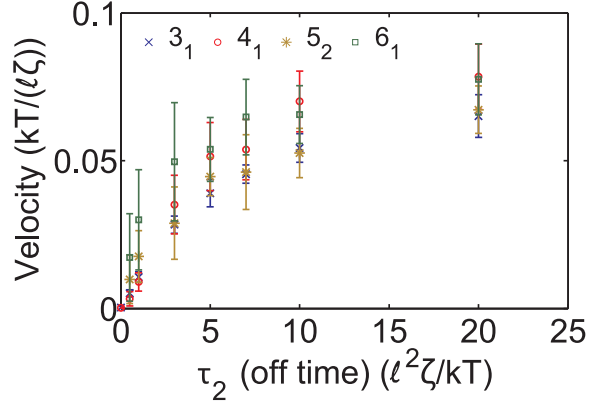


Figure S8: Topology dependence of translocation speed under a pulsed force field. We cycle the force between $f_1 = 7 kT/\ell$ and $f_2 = 0 kT/\ell$, and we set the total cycle time to be $\tau_1 + \tau_2 = 100 \ell^2 \zeta/kT$. The force f_1 is such that the knot jams at the pore entrance but swells normally during the relaxation cycle. The bead size is equal to the rod length ($b = \ell$).

touching beads ($b = \ell$), non-touching beads ($b = 0.8\ell$), and overlapping beads ($b = 1.5\ell$).

Fig S9 plots the translocation speed of the 3_1 and 4_1 knots when they move through a pore under constant force. The pore radius is $R = 0.8\ell$ for Fig S9a, and the pore radius is $R = 1.0\ell$ for Fig S9bc. In Fig S9a, we see that the knot jams at lower forces when the backbone is more corrugated ($b = 0.8\ell$ compared to $b = \ell$). When the polymer backbone is fairly smooth ($b = 1.5\ell$), the jamming behavior depends greatly on the topology of the chain. For example, we do not observe jamming for the 3_1 knot over the force range studied (Fig S9b), but we observe jamming for the 4_1 knot for forces $f \geq 20kT/\ell$ (Fig S9c). Traces of polymer trajectories show that the 4_1 knot jams in a multi-step process when the polymer backbone is smooth ($b = 1.5\ell$). This behavior contrasts to case of touching beads ($b = \ell$) where the polymer jams when the knot first contacts the pore (see Fig 2a in main text).

In Fig S10, we examine how the corrugation along the backbone affects the relaxation behavior of a knot. We simulate a 3_1 and 4_1 -knotted polymer undergoing a step-relaxation at the pore wall. The initial force on the chain is well above the knot's jamming transition, and we track the knot size as a function of time after the field is turned off. When the

polymer backbone consists of non-touching beads ($b = 0.8\ell$), we observe an enhancement of the topology-dependent caging phenomenon described in the main text. The 3_1 knot swells normally during relaxation (Fig S10a), but almost all of the 4_1 knots fail to unjam (Fig S10a). We suspect that similar caging will occur for all other non-torus topologies as well. When the polymer backbone is fairly smooth ($b = 1.5\ell$), we find that all knots swell even at very large initial forces (fig S10c). Thus, glassy dynamics are suppressed for smooth backbones since the escape potential is much less than kT .

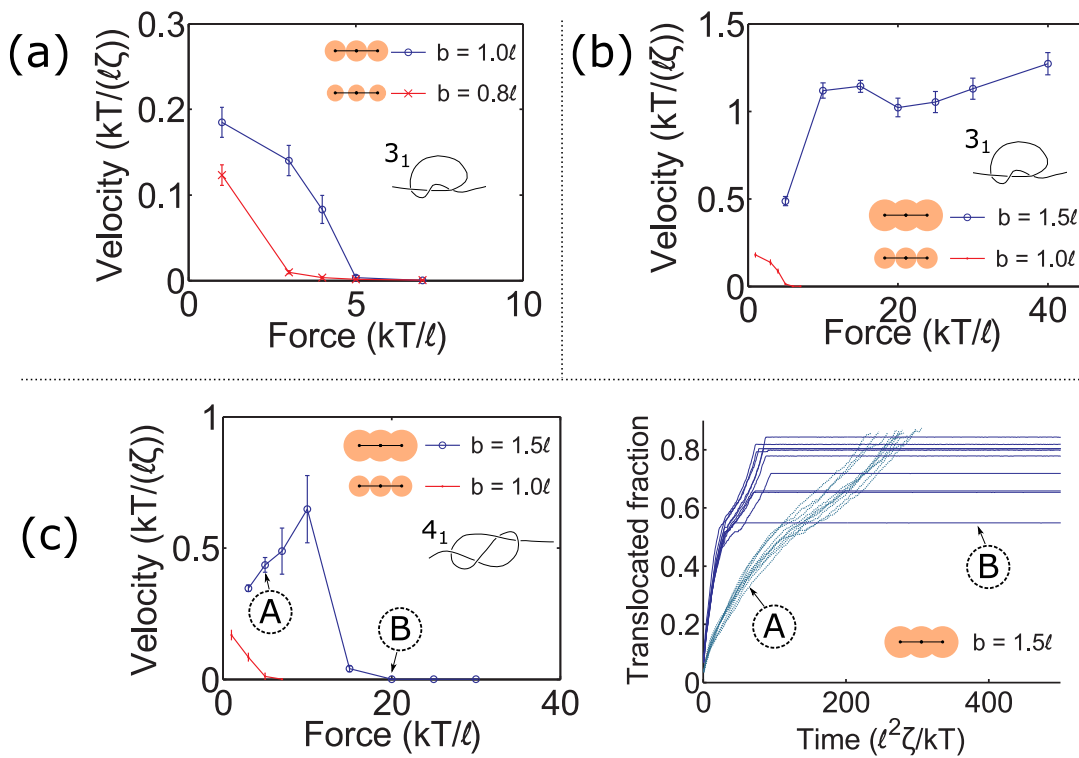


Figure S9: Effect of polymer backbone corrugation on the jamming behavior of knots at the pore entrance. (a) Translocation speed of a 3_1 knot through a pore of radius $R = 0.8\ell$. We examine two different corrugations: touching beads ($b = \ell$) and non-touching beads ($b = 0.8\ell$). (b) Translocation speed of a 3_1 knot through a pore of radius $R = 1.0\ell$. The corrugations we examine are touching beads ($b = \ell$) and overlapping beads ($b = 1.5\ell$). (c) Same as (b) except that we examine the 4_1 knot. Traces of polymer trajectories show that jamming occurs in a multi-step process for the smoother polymer backbone ($b = 1.5\ell$). The translocation speed plotted on the left hand side reflects the speed during the final stage of motion.

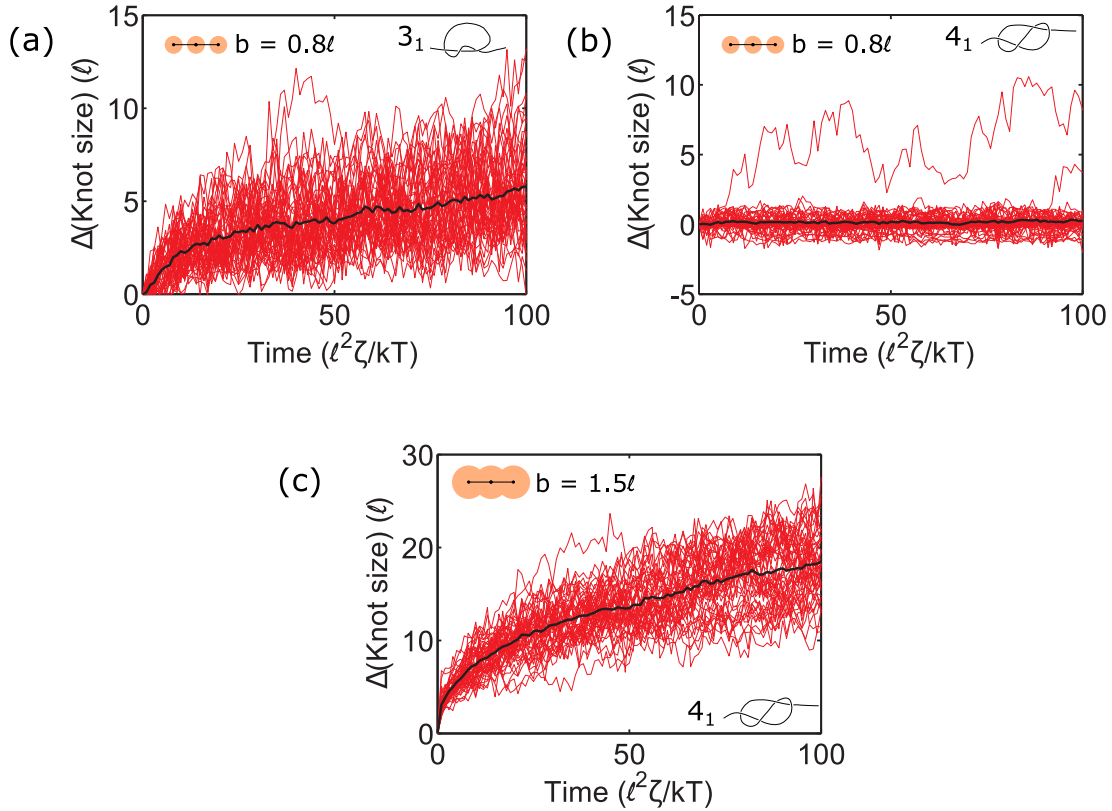


Figure S10: Step relaxation of knotted polymers with different backbone corrugations. (a) 3_1 knot with non-touching beads ($b = 0.8\ell$). The pore radius is $R = 0.8\ell$ and the initial force before relaxation is $f = 5kT/\ell$. (b) 4_1 knot with non-touching beads ($b = 0.8\ell$). The pore radius is $R = 0.8\ell$ and the initial force before relaxation is $f = 5kT/\ell$. (c) 4_1 knot with overlapping beads ($b = 1.5\ell$). The pore radius is $R = 1.0\ell$ and the initial force before relaxation is $f = 40kT/\ell$.

Model for translocation velocity

In this section, we provide insight into how the polymer ratchets through the pore. Suppose we cycle the force field between two values: $f_1 = f$ and $f_2 = 0$, where f is above the jamming transition of the knot. There are two contributions to the stair-step translocation profiles as seen in Fig 4c in the main text. During the off cycle, the knot swells and diffuses away from the pore, which allows contour to reptate into the left hand side of the knot (provided the polymer moves left to right). When the force is turned back on, additional contour can reptate through the knot as it tightens. Let $\Delta\ell_{left}$ be the contour that moves into the left boundary of the knot during relaxation, and let Δs be distance between the pore wall and the right entrance of the knot after relaxation (Fig S11). When the force turns back on, the time it takes for the knot to contact the pore again is $\Delta t = \zeta\Delta s / f_{tot}$, where $f_{tot} = (L/\ell)f$ is the total force on the chain. During this time, the additional contour that reptates through the knotted core is $\Delta x_{knot} = \Delta t f_{tot} / \zeta_{knot} = \Delta s \cdot (\zeta / \zeta_{knot})$. Thus, the total contour that goes through the knot during one cycle is:

$$\ell_{rep} = \Delta\ell_{left} + \Delta s \cdot (\zeta / \zeta_{knot}) \quad (10)$$

We expect the friction ratio $\zeta / \zeta_{knot} < 1$ as it is more difficult to reptate through the knotted core than free space. However, since the knot is swollen at the end of relaxation, we expect ζ / ζ_{knot} to be an $O(1)$ quantity. We can test this physics by performing step relaxation simulations of knots (Fig S7) to obtain $\Delta\ell_{left}$ and Δs during the relaxation cycle. We estimate the average translocation speed per cycle $\langle v \rangle = \ell_{rep} / \tau_{cycle}$ and compare it to the actual translocation speed using the friction ratio ζ / ζ_{knot} as a free parameter. We obtain good agreement with the actual translocation speed when the friction parameter is $\zeta / \zeta_{knot} \approx 0.69$ for both the 3_1 and 5_1 knots (Fig S11). Thus, the physical picture we present here is consistent with what is observed and could be used in the future to develop predictive models for the ratcheting dynamics.

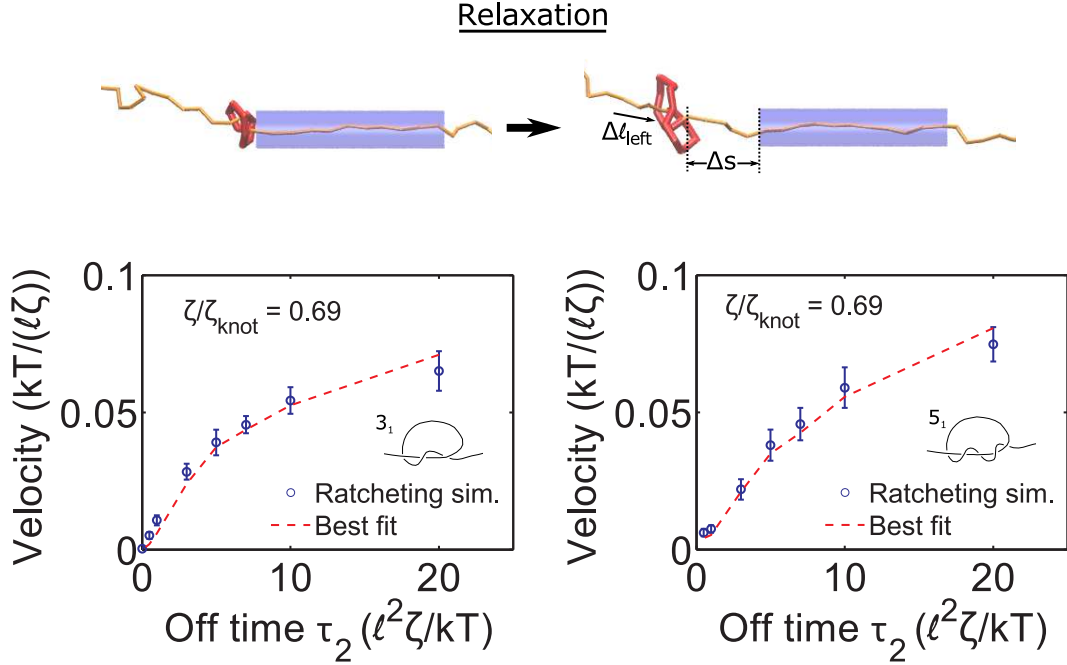


Figure S11: Comparison between model and simulations for ratcheting dynamics. *Top:* When a knot relaxes, it swells and diffuses away from the pore. The quantities $\Delta\ell_{left}$ and Δs are the amount of contour that reptates into the knot's left side and the distance between the pore and the right side of the knot, respectively. *Bottom:* Using eqn (10), we estimate the translocation speed of the polymer using $\Delta\ell_{left}$ and Δs calculated from step-relaxation simulations. We compare these results to simulations where we ratchet the polymer with a field that turns on and off. For the 3_1 knot, the parameters for the ratcheting simulations are: $f_1 = 7kT/\ell$, $f_2 = 0$, $\tau_1 + \tau_2 = 100 \ell^2\zeta/kT$. For the 5_1 knot, the parameters are: $f_1 = 15kT/\ell$, $f_2 = 0$, $\tau_1 + \tau_2 = 100 \ell^2\zeta/kT$.

Movies

Below we describe the movies included in the supporting info. In these videos, we color the knotted region red. This region is determined by calculating the smallest subset of the chain that retains its topology via computation of the Alexander polynomial (see Methods). For illustration purposes, we do not show the planar wall of the pore and the beads on the bead-rod chain.

- 4_1_f3.mpg – This movie shows a 4₁-knotted polymer moving through a pore when the external field is constant ($f = 3 kT/\ell$). The bead size is equal to the rod length ($b = \ell$). Here, the polymer translocates at a nearly uniform speed.
- 4_1_f5.mpg – This movie shows a 4₁-knotted polymer moving through a pore when the external field is constant ($f = 5 kT/\ell$). The bead size is equal to the rod length ($b = \ell$). Here, the polymer moves in a stick-slip fashion.
- 4_1_f7.mpg – This movie shows a 4₁-knotted polymer moving through a pore when the external field is constant ($f = 7 kT/\ell$). The bead size is equal to the rod length ($b = \ell$). Here, the knot jams at the pore entrance and halts translocation.
- 3_1_f7_f0_t80.mpg – This movie shows a 3₁-knotted polymer ratcheting through a pore when the field cycles on and off at values $f_1 = 7 kT/\ell$ and $f_2 = 0 kT/\ell$. The cycle times are $\tau_1 = 80\ell^2\zeta/kT$ and $\tau_2 = 20\ell^2\zeta/kT$. The bead size is equal to the rod length ($b = \ell$).
- knot4_1_relax_swell.mpg – This movie shows a step-relaxation simulation of a 4₁-knotted polymer. Here, the knot swells normally during relaxation. The initial force is $f = 15 kT/\ell$ and the bead size is equal to the rod length ($b = \ell$).
- knot4_1_relax_no_swell.mpg – This movie shows a step-relaxation simulation of a 4₁-knotted polymer. Here, the knot gets trapped in a metastable state during

relaxation. The initial force is $f = 15 kT/\ell$ and the bead size is equal to the rod length ($b = \ell$).

References

- (1) Heyes, D. M.; Mitchell, P. J.; Visscher, P. B.; Melrose, J. R. *J. Chem. Soc. Faraday Trans.* **1994**, *90*, 1133–1141.
- (2) Somasi, M.; Khomami, B.; Woo, N. J.; Hur, J. S.; Shaqfeh, E. S. G. *J. Non-Newtonian Fluid Mech.* **2002**, *108*, 227–255.
- (3) Boyd, S.; Vandenberghe, L. *Convex Optimization*; Cambridge Univ. Press, 2009; Vol. 7.
- (4) Pasquali, M.; Morse, D. C. *J. Chem. Phys.* **2002**, *116*, 1834–1838.
- (5) Hinch, E. J. *J. Fluid Mech.* **1994**, *271*, 219–234.
- (6) Scharein, R.; Ishihara, K.; Arsuaga, J.; Diao, Y.; Shimokawa, K.; Vazquez, M. *J. Phys. A: Math. Theor.* **2009**, *42*, 475006.
- (7) Wall, F. T.; Mandel, F. *J. Chem. Phys.* **1975**, *63*, 4592.
- (8) Vologodskii, A. V.; Lukashin, A. V.; Frank-Kamenetskii, M. D.; Anshelevich, V. V. *Zh. Eksp. Teor. Fiz.* **1974**, *66*, 2153–2163.
- (9) Virnau, P. *Phys. Procedia* **2010**, *6*, 117–125.
- (10) van Dorp, S.; Keyser, U. F.; Dekker, N. H.; Dekker, C.; Lemay, S. G. *Nat. Physics* **2009**, *5*, 347–351.
- (11) Behrens, S.; Grier, D. *J. Chem. Phys.* **2001**, *115*, 6716–6721.